

See discussions, stats, and author profiles for this publication at: <https://www.researchgate.net/publication/51583097>

Detection of Weak Absorption Changes from Molecular Events in Time-Resolved FT-IR Spectromicroscopy Measurements of Single Functional Cells

ARTICLE *in* ANALYTICAL CHEMISTRY · AUGUST 2011

Impact Factor: 5.64 · DOI: 10.1021/ac201318z · Source: PubMed

CITATIONS

19

READS

70

3 AUTHORS, INCLUDING:



Luca Quaroni

Institute of Nuclear Physics

84 PUBLICATIONS 1,017 CITATIONS

[SEE PROFILE](#)



Elise Normand

University of Saskatchewan

2 PUBLICATIONS 22 CITATIONS

[SEE PROFILE](#)

Detection of Weak Absorption Changes from Molecular Events in Time-Resolved FT-IR Spectromicroscopy Measurements of Single Functional Cells

Luca Quaroni,^{*†} Theodora Zlateva,[‡] and Elise Normand[§]

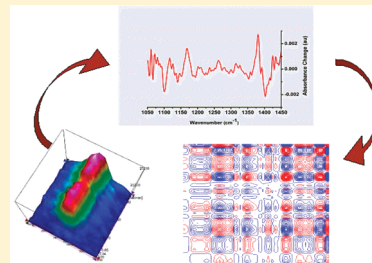
[†]Swiss Light Source, Paul Scherrer Institut, 5232, Villigen-PSI, Switzerland

[‡]Department of Biochemistry and Cancer Research Center, University of Saskatchewan, Saskatoon, SK, S7N 5E5, Canada

[§]Canadian Light Source Inc., University of Saskatchewan, Saskatoon, SK, S7N 0X4, Canada

 Supporting Information

ABSTRACT: The possibility of performing FT-IR spectromicroscopy experiments on individual living cells is the focus of considerable attention. Among the applications of interest, the obtainment of structural information in rapid measurements, with a time resolution of the minute or better, is a prized goal. In this work, we show that the use of synchrotron FT-IR spectromicroscopy allows one to extract weak spectral changes, of less than 10^{-3} au per minute, in the absorption spectrum of single rod cells following photostimulation. We also show that absorption changes are accompanied by other optical effects due to changes in the real part of the refractive index of the cell. The use of two-dimensional correlation spectroscopy allows us to assign bands to specific molecular chromophores and to extract weak spectral variations in the presence of a noisy background.



Fourier-transform infrared (FT-IR) spectroscopy is a helpful technique for the study of biological molecules, due to its sensitivity to molecular structure and conformation and its usefulness in studying reaction mechanisms.^{1–3} Experiments using FT-IR spectroscopy are usually performed with partially or fully purified biomolecules, often reconstituted under conditions that mimic some features of their native cellular environment, and with sample size on the order of a few millimeters. Although this approach has been very successful, it still suffers from the intrinsic limitation that conclusions from such studies *in vitro* are then used to extrapolate biochemical behavior *in vivo*.

The introduction of optical configurations for FT-IR spectromicroscopy has allowed the measurement of spectra of samples of less than a millimeter in size and opened the possibility of performing studies using intact tissue and cells while selectively probing specific regions of the sample.^{4–6} The use of synchrotron IR light sources has allowed these experiments to be extended to samples requiring diffraction limited spatial resolution.^{7,8} This success has been used for qualitative analysis of cellular composition, to identify the presence of general classes of biomolecules, such as proteins and lipids, and map their subcellular distribution,⁹ even in physiologically relevant aqueous suspensions.¹⁰ More recently, a new beamline design has been introduced to allow rapid full-field imaging of biological samples with synchrotron IR light.^{11,12} We are now aiming to progress beyond the state-of-the-art by evaluating the performance of the technique in structure–function studies of specific biomolecules *in vivo*. In previous work, we have shown the viability of single-cell vibrational linear dichroism

measurements using synchrotron FT-IR spectromicroscopy to assess the order parameters of molecular components in individual retinal rod cells.¹³ In addition, we have shown that FT-IR spectromicroscopy with synchrotron light provides sufficient signal-to-noise (S/N) ratios to measure in real time the formation of small molecule metabolites in a single algal cell with a time resolution on the order of the minute.¹⁴ We are now testing the viability of sensitive and selective time-resolved studies on individual retinal rod cells.

Retinal rod cells are a well-studied system, providing a wealth of comparative information and making them a useful benchmark to test the viability of subcellular spectromicroscopy and to develop measurement and data analysis protocols optimized for the purpose. Rod cells are responsible for vision under conditions of weak illumination.^{15–17} They are composed of an inner segment (Rod Inner Segment, RIS) portion, which is the site of cellular metabolism, and an outer segment (Rod Outer Segment, ROS) containing the molecular machinery involved in photo-transduction. The composition of the ROS is relatively simple, facilitating an FT-IR investigation. Although the overall number of molecular species is elevated, only few components are present at sufficiently high concentration to be appreciated by a transmission FT-IR measurement. The protein complement is dominated by the photoreceptor protein rhodopsin (Rho).^{18,19} Less abundant proteins include transducin and arrestin.^{20,21}

Received: May 24, 2011

Accepted: August 19, 2011

Published: August 19, 2011

Other proteins are at concentrations below the detection limit of the technique. In contrast to composition, the morphology of rod cells is challenging for a spectromicroscopy measurement. Amphibian rod cells are elongated cells where the ROS is a cylinder 30–50 μm long and 4–7 μm in diameter. Mammalian rod cells are even smaller, with ROS diameter typically of 1–2 μm . Because of the small transversal diameter, a few micrometers, single cell spectromicroscopy measurements must be performed at or close to the diffraction limit, even for the larger amphibian ROS, when mid-infrared radiation is used.

FT-IR measurements in single rod cells rely on concentrations of Rho and lipids that are similar to the ones used for in vitro experiments,²² suggesting that comparable sensitivity can be achieved. The detection and assignment of infrared absorption bands from some chromophores and the observation of their time evolution following stimulation by light can open the way to the study of correlations between multiple molecular events in an intact cell.

In this work, we show that FT-IR spectromicroscopy with synchrotron radiation (SR-FT-IR) allows us to reach this objective, by providing time-resolved spectra with high signal-to-noise following photoexcitation of individual functional cells. In addition, we show that two-dimensional (2D) correlation spectroscopy is a powerful tool in clarifying the resulting complex spectral changes and in identifying specific chromophores.

■ EXPERIMENTAL METHODS

All chemicals were purchased from Sigma (St. Louis, MO, USA) and were of the highest grade available, except when noted below. *Bufo marinus* toads were purchased from Boreal Laboratories (Quebec, Canada) and kept at the Animal Care Unit at the University of Saskatchewan (UCACS Protocol Number 20070030, to Luca Quaroni). The animals were allowed to acclimate for at least two weeks and maintained under cyclic lighting (12 h light, 12 h dark) prior to use. On the day before the experiment, the animals were dark adapted overnight and moved to the beamline inside a light tight box. The animals were euthanized by decapitation and pithing under dim red light, and the eyes were removed and sectioned. Retinas were dissected free of pigment epithelium and gently shaken in chilled Ringer's solution (NaCl, 80 mM; KCl, 2 mM; CaCl₂, 0.1 mM; MgSO₄, 0.1 mM; NaH₂PO₄/Na₂HPO₄, 12.5 mM) to shed rod cells. The cell suspension was transferred to a custom-made holder for FT-IR measurements in aqueous environment, fitted with two 25 mm CaF₂ optical windows separated by a 5 μm PTFE spacer.

For such measurements, the condenser of the microscope was aligned to maximize throughput in the 1000–1800 cm^{-1} spectral region. Due to the high level of chromatic aberration introduced by the CaF₂ optical windows of the sample holder, this alignment implies that throughput at shorter wavelengths is sacrificed, with correspondingly higher noise levels above 1800 cm^{-1} . As a consequence and also because of the high absorption from the water stretching band around 3400 cm^{-1} , spectral traces in the region between 2700 cm^{-1} and 3600 cm^{-1} provide insufficient signal-to-noise ratio and are not reported.

Synchrotron FT-IR spectromicroscopy measurements were performed on the endstation of beamline 01B1-1 at the Canadian Light Source, using a Bruker IFS66 v/S (Bruker Optics, Billerica, MA, USA) interferometer coupled to a Bruker Hyperion 2000 microscope, and on the endstation of beamline X01DC of the Swiss Light Source, using a Bruker Vertex 70

interferometer coupled to a Bruker Hyperion 2000 microscope. For these measurements, a KBr-supported Ge-multilayer beamsplitter was used together with a liquid nitrogen-cooled MCT detector. The interferometer was scanned with an acquisition rate of 40 kHz with 4 cm^{-1} resolution. 64 scans were collected for each time point; points were spaced 15 s. Measurements were performed in transmission. Single channel spectra (SSc) were obtained by performing a Fourier Transform of the interferogram after apodization with a Blackman-Harris 3-Term function, using no zero-filling and a Mertz phase correction. The confocal blades of the microscope were set at 20 \times 20 m^2 for the lower aperture and 5 \times 12 m^2 for the upper aperture. The confocal apertures of the IR microscope were centered on the ROS of a single cell using deep red and near-infrared illumination ($\lambda > 700 \text{ nm}$). The rectangular upper aperture was centered on the outer segment of a rod cell and rotated to align with the axis of the segment. Illumination was turned off, and the cell was then allowed to adapt to full darkness for at least 5 min. During this time, transmitted mid-infrared light was recorded continuously. The cell was then exposed to intense white light from a 100 W halogen lamp for 60 s. Measurements were continued without interruption, during illumination and afterward, for 30 min or longer. Exposure to visible light is carried out by switching the microscope optical path between the one used for the IR light and the one used for visible light while performing repeated rapid scans. This interrupts the recording of IR light by the detector and leads to a sharp and complete drop of intensity in the SSc trace, followed by a sharp recovery after the optical path for IR light is re-established. If the switching of the mirror happens to be performed in the course of a scan, the scan is ignored and the intensity of IR light is set to zero for that scan, to avoid the plotting of scans with only partial exposure.

Conventional FT-IR measurements of retinal solutions were performed on a Bruker Vertex70 interferometer coupled to a Bruker Hyperion 3000 microscope. A solution of the retinal was enclosed between two micromachined CaF₂ optical windows with a 6 μm deep round indentation²³ and positioned on the stage of the FT-IR microscope. Measurements were performed in transmission using a KBr supported Ge multilayer beamsplitter and a liquid nitrogen-cooled MCT detector. The interferometer was scanned with an acquisition rate of 40 kHz at 4 cm^{-1} resolution. 64 scans were collected for each spectrum, with one spectrum measured every 15 s. Single channel spectra were obtained by performing a Fourier Transform of the interferogram after apodization with a Blackman-Harris 3-Term function, using no zero-filling and a Mertz phase correction.

Spectral analysis, curve fitting, and diagram preparation were performed using Origin 8.0. (OriginLab, Northampton, MA, USA) Curve fitting was performed using a nonlinear fit to an exponential function of the form $y = y_0 + A_1 e^{-(x)/(t_1)} + A_2 e^{-(x)/(t_2)}$ to the SSc trace.

Generalized two-dimensional (2D) correlation analysis was performed using the Mid-Infrared Data Analysis Software (MIDAS, Elise Normand, University of Saskatchewan, Saskatoon, SK, Canada) package, implemented in Matlab (Mathworks, Natick, MA, USA). MIDAS is a graphical interface which, aside from the regular Matlab tools and utilities, transforms the data into the Fourier domain along the dynamic variable and calculates the cross correlation. Two-dimensional correlation analysis performs a univariate correlation analysis on all the variable combinations.²⁴ Synchronous and asynchronous correlation

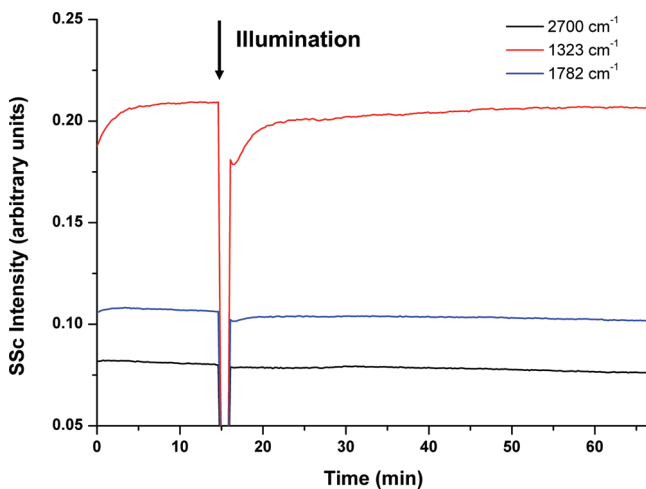


Figure 1. Changes in intensity following photoexcitation. Changes in the total light intensity (SSc intensity) crossing a single ROS and measured at the detector following photoexcitation. The changes are shown at three different wavenumber values, 2700 cm^{-1} , 1323 cm^{-1} , and 1782 cm^{-1} . The notch at about 15 min corresponds to the period of illumination with visible light from a halogen lamp, as indicated, during which the IR beam is interrupted. Time $t = 0$ corresponds to the first measurement after centering the cell under red light and turning the light off. An exponential stabilization process is observed both after illumination with red light and after illumination with intense white light.

plots are produced by extracting the real and imaginary components from the resulting cross correlation matrix. Additionally, the program allows various preprocessing algorithms, such as removal of static components, and filtering of the data so as to eliminate high frequency noise.

■ RESULTS AND DISCUSSION

We have measured changes in the mid-infrared (mid-IR) absorption spectrum of individual rod cells following one minute of exposure to intense visible white light. Measurements were performed using a suspension of cells in Ringer solution, as described in the Experimental Methods section, so as to provide environmental conditions which are as close as possible to the ones used for conventional measurements of rod physiology.

Changes in Total Transmitted Intensity. Exposure of rod cells to light induces time dependent changes in the intensity of the single channel spectrum (SSc) over the spectral range $1000\text{--}1800\text{ cm}^{-1}$. Figure 1 shows this evolution before photoexcitation and over the time course of 60 min following photoexcitation. The SSc spectrum represents the total light intensity as recorded by the detector. Therefore, it is a measure of light throughput along the optical system and across the sample itself. Illumination with visible light shuts off the IR beam, as described in the Experimental Methods section, and gives rise to the sharp drop at 15 min followed by a sharp increase when visible illumination is stopped. After interruption of illumination, the SSc trace shows a progressive drop of total intensity over part of the mid-IR spectral range. The decrease progresses for about 30 s after discontinuing illumination and is followed by an asymptotic recovery of the initial intensity over the course of a few minutes. The amplitude of the changes is larger around 1320 cm^{-1} and minimal at the extremes of the spectral range. No changes are observed above 2000 cm^{-1} ,

except for a slow decrease of intensity corresponding to current decay in the storage ring.

The recovery phase can be fit to two exponential phases with time constants $t_1 = 8.56$ (0.255) min and $t_2 = 86.9$ (6.73) min (Figure 1). The initial decrease is sampled by three experimental time points only, preventing a meaningful fitting to a third exponential. Its time constant (t_0) can be just estimated to be less than 1 min. The amplitude of these changes is variable from cell to cell, with the trace in Figure 1 showing the wider end of the response range. Rod cells and ROS that appear intact under visual inspection provide wider changes, whereas fragments provide a weak response or no response at all.

A brief exponential recovery is also seen for a few minutes at the very beginning of the measurement. We attribute these changes to stimulation of the ROS during sample inspection and alignment. The microscope visible light source is filtered during this preparatory activity so that only deep red and near IR light is focused on the sample. Nonetheless, it cannot be ruled out that there is some weak exposure of the ROS to other regions of the visible spectrum, caused by the weak background of scattered light within the microscope itself that is picked up by the optics and directed onto the sample. The length of the exposure required to locate and align a ROS coupled to the sensitivity of ROS to weak illumination would be sufficient to observe stimulation.

ROSs are known to undergo changes in structure and refractive index following stimulation by visible light.^{25,26} The associated anomalous dispersion effect has been used to interpret polarization dependent variations in the scattering of near-IR light following photoexcitation. Such refractive index changes can be positive or negative and occur over a time scale that ranges from milliseconds to minutes. In accordance, we propose that the variations in single channel traces observed in our experiments are also consistent with the same optical interpretation; namely, they arise from changes in the real part of the refractive index of the cell as a consequence of photoexcitation. The near-IR spectral range is the region where overtone absorptions from vibrational transitions occur, while our experiments probe the mid-IR spectral region, corresponding to the fundamental transitions associated to normal modes in ROS molecules. Absorption bands in the mid-IR region are also associated to variations in the real refractive index and give rise to anomalous dispersion.^{27–29} The change in intensity reported in Figure 1 does indeed correspond to the $1000\text{--}1800\text{ cm}^{-1}$ spectral region, where a high density of absorption bands from the molecular components of the ROS is present. A photoexcitation-induced variation of the real refractive index can perturb the propagation of mid-IR light through the ROS by varying either the scattering cross-section and/or the refraction geometry of the IR beam. The effect of the sample refractive index and its geometry in an FT-IR spectromicroscopy measurement has been described in detail by Bhargava et al.^{27,28} A small perturbation of beam geometry easily results in a net variation of the intensity crossing the confocal apertures and reaching the detector, reflected in turn in wavenumber dependent variations of spectral intensity of the single channel trace. Recently, the effect of cylindrical sample geometry on the shape of absorption spectra in the mid-IR spectral region has been addressed using classical optical theory.²⁹ According to this treatment, large changes in the transmission of mid-IR light are expected when varying the radius of a cylindrical sample, caused by refraction and scattering of light. These changes are maximal in spectral regions where the cylinder absorbs and at wavelengths

that are close to the radius of the cylinder. Very little changes are observed between 2000 cm^{-1} and 2700 cm^{-1} . Rod cells from *Bufo marinus* range from 6 to 8 μm in size, corresponding to 1700 cm^{-1} to 1250 cm^{-1} . This is in qualitative agreement with our observations, where the maximum change in the SSc trace is observed around 1320 cm^{-1} but drops off at higher photon energy.

Changes in the geometry or refractive index of the ROS following photoexcitation of the retina have been shown to affect micro attenuated total reflection measurements (micro-ATR).³⁰ With the current experiments, we are now showing that these changes arise at the level of the single cell. The confocal geometry used in our measurements, with a sharply focused beam and field apertures closed down to values at the diffraction limit, is particularly sensitive to variations in beam propagation.²⁸

Several events induced by photoexcitation are known to occur in the ROS on a time scale comparable to the processes reported in Figure 1 and provide insight into the molecular or physiological changes underlying variations in refractive index. Light-induced relocation of the G-protein transducin from the inner to the outer segment of retinal receptors gives rise to changes in the FT-IR absorption spectrum over this time scale, as detected by micro-ATR.³⁰ Some of the spectral changes have also been related to a reorganization of ROS geometry. The electrophysiological response of single amphibian ROS displays a similar time dependence.³¹ Recovery of the dark adapted, prebleaching state occurs according to an exponential process, with a time constant $t = 9\text{ min}$, closely matching the value of t_1 from our measurements of infrared throughput recovery after bleaching. These kinetics have been related to the accumulation and subsequent decay of the meta-II and meta-III intermediates of the rhodopsin photocycle, accompanied by release of all-trans-retinal from Rho. In particular, accumulation of meta-III is expected to dominate relaxation processes on the slowest time scales. Visible light absorption measurements of individual amphibian rod cells following photobleaching³² confirm that the overall decay of meta-II and meta-III to opsin and free retinal takes place over the course of 30 min, with an average time constant of approximately 10 min, in agreement with the time of recovery of infrared throughput observed in our experiments, as well as with electrophysiology measurements.³¹ Electroretinography (ERG) experiments on whole mouse retinas³³ showed a response with similar time constants and were interpreted in terms of Rho dephosphorylation dominating the slower processes, over the course of 30 to 60 min after exposure to bright light.³³ The structure of lipid membranes within the ROS is also subject to variations on the time scale of minutes following photoexcitation,³⁴ with rapid phospholipid reorganization induced by photoexcitation followed by a slow recovery process of 10–20 min. On the basis of the similarity of kinetics, we propose that the recovery process in electrophysiological measurements and the associated decay of meta-II and meta-III contribute to the process described by t_1 . In contrast, the process described by t_2 is dominated by rhodopsin dephosphorylation, lipid reorganization, and transducin relocation.

Changes in the Absorption Spectrum. To obtain detailed information on molecular events occurring in single rod cells, we examined the changes in mid-IR absorption following photoexcitation. Differential absorption spectra as a function of time were obtained by referencing single channel traces recorded after excitation to traces recorded in the dark. As expected, the illumination and time dependent variations in optical properties

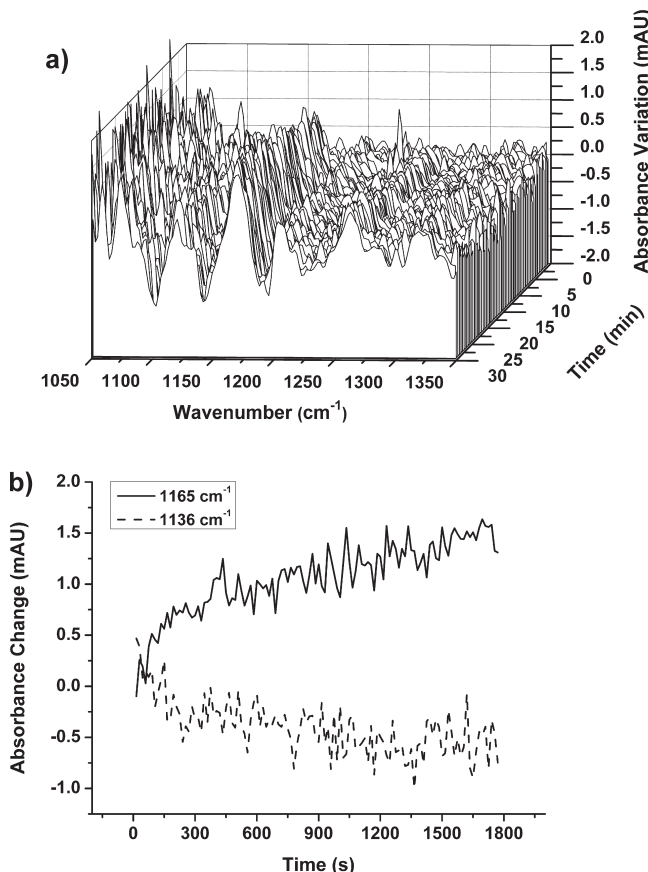


Figure 2. Changes in differential absorbance after photoexcitation. Panel a shows the evolving absorption spectra in the “retinal fingerprint” region following photoexcitation of a ROS obtained after detrending. Spectra were measured every 15 s. Difference spectra are calculated by subtracting a spectrum recorded just before illumination and shown evolving over a period of 30 min. Several absorbance variations on the order of 10^{-3} au can be appreciated over the course of a few minutes. Panel b shows the change of absorbance at 1165 cm^{-1} and 1136 cm^{-1} extracted from the spectra in panel a.

reported in Figure 1 give rise to major changes in the baseline of differential absorption spectra recorded after photoexcitation (see Supporting Information). These baseline variations are time and frequency dependent and hinder plotting of pure absorbance changes as a function of time. To overcome this limitation, we developed an unsupervised protocol to detrend the spectra while limiting subjective choices in background subtraction. The protocol is described in the Experimental Methods section. To ensure minimal interference from water vapor absorption, only the kinetics in the spectral region below 1500 cm^{-1} are analyzed quantitatively using this algorithm. The detrended spectrum shows weak but clear changes in absorption occurring over the mid-IR spectral region as a pattern of positive and negative bands (Figure 2a) developing over the course of 30 min after exposure to light. Spectra are reported as absorbance changes relative to a measurement recorded just before illumination and represent the range of slow processes that occur when the system relaxes after photoexcitation. Between 1100 cm^{-1} and 1400 cm^{-1} , noise levels for one-minute measurements range from 1×10^{-4} to $5 \times 10^{-4}\text{ au}$. When the convention of accepting peaks of intensity at least three times higher than noise is followed, the observed noise levels allow the detection of absorbance changes of 3×10^{-4} to

1.5×10^{-3} au. The Lambert–Beer Law can be used to estimate the concentration of chromophores that is observable. Using typical extinction coefficients for small organic molecules (e.g., about $0.1\text{--}0.01 \text{ M}^{-1} \mu\text{m}^{-1}$ for a methyl stretching vibration in a short-chain alcohol³⁵), we can estimate that the accessible absorbance range allows one to detect molecular chromophores at concentrations as low as mM with an optical path on the order of $10 \mu\text{m}$. Figure 2b shows the time-resolved traces extracted from the spectra in Figure 2a, representing absorbance changes at 1165 cm^{-1} and 1136 cm^{-1} . Even for these 15 s measurements, the quality of the traces is such to easily allow extracting time constants for the corresponding molecular changes. The possibility of extracting such plots opens the way to quantitative kinetic studies of cellular transformations.

Most *in vitro* studies of Rho photointermediates based on FT-IR spectroscopy rely on the observation of absorption changes between 1300 cm^{-1} and 1800 cm^{-1} , dominated by the spectroscopic features of the protein. It is customary to identify specific intermediates on the basis of their absorption pattern in difference spectra recorded following excitation.³⁶ In our measurements, the combined effects of water absorption and changes due to protein relocation and to the presence of carbonylic, aromatic, and polyenic compounds, plus possible residual absorption from water vapor in the atmosphere, prevent specific band assignments of the spectral variations observed between 1500 cm^{-1} and 1700 cm^{-1} . In contrast, a simpler pattern of changes is observed in the $1050\text{--}1500 \text{ cm}^{-1}$ interval, which is commonly called the “chromophore fingerprint” region. Modes of the retinal chromophore that have been used to characterize the isomeric state and the conformation of the chromophore appear in this region.²³ The position of retinal vibrational bands has been calculated and/or measured for several intermediate states of the rhodopsin photocycle using either FT-IR or Raman spectroscopy.^{23,37,38} Important contributions to this region also arise from bands of phosphoryl-containing chromophores, such as phospholipids, nucleotides, and phosphorylated proteins. The time scale of our observation is on the order of minutes, and only the slowest evolving processes and intermediates are expected to be present in significant concentrations for an FT-IR measurement. Therefore, the dominant contributions are expected to arise from phosphoryl groups in the cell and intermediates meta-II and meta-III, plus dark adapted Rho, and free all-trans retinal.³⁹ The concentration of Rho in amphibian cells has been quantified at $2\text{--}3 \text{ mM}$,^{18,19} similar to the protein concentration in samples used for *in vitro* measurements. At this concentration, the absorbance changes of Rho and its retinal cofactor induced by photoexcitation are expected to be on the order of $10^{-2}\text{--}10^{-3}$ au in the amide region and $10^{-3}\text{--}10^{-4}$ au in the retinal fingerprint region,^{40,41} in the same range as the absorption values that we report in our measurements.

Comparison with band frequencies reported from measurements on purified proteins^{36,40,41} suggests that in the spectral range of Figure 2a spectroscopic contributions from some slowly evolving Rho intermediates may be present. Additional contributions may arise from nonprotein chromophores that are abundant in the ROS. The fraction of Rho that is phosphorylated and dephosphorylated is between 0.30 and 0.80, with sufficient change in phosphoryl concentration to produce FT-IR absorbance changes of 10^{-4} au in the region between 900 and 1300 cm^{-1} . The largest contribution from phosphoryl absorption is expected to arise from the headgroups of phospholipids, which constitute about 50% of the mass of the ROS, contributing

an average concentration of phosphoryl groups on the order of the 100 mM .⁴² Changes in the absorption of lipids are expected due to disk swelling²⁶ and lipid relocation⁴³ following excitation. Similarly, contributions are also possible due to variations of cellular concentrations of ATP, ADP, and phosphocreatine.

2D Correlation Spectroscopy and Chromophore Identification. The difference spectra in Figure 2a,b provide a comparatively high signal-to-noise ratio for a diffraction-limited measurement on the time scale of the minute. Nonetheless, the raw spectra are themselves not amenable to inform on the structural dynamics of the chromophores, due to the complexity of the spectrum recorded at each time point. Such analysis requires the capability to resolve and assign bands from the different molecular species evolving in the system.

We have utilized 2D correlation analysis to help with band assignment to specific chromophores. 2D correlation analysis was introduced by Noda⁴⁴ as a tool to analyze the spectra of complex evolving systems. A detailed description of 2D correlation analysis is beyond the scope of this work, and the reader is directed to a recent monograph and several reviews for a detailed description of its features. Here, it will suffice to highlight that the analysis provides a quantitative assessment of the phase relationship existing between the evolving bands of chromophores in the sample, allowing its parametrization and use in a systematic analysis. In an application to the study of the molecular response of the retina, Massaro et al.³⁰ showed that the analysis is useful in the identification of bands arising from the same molecular chromophore even in the presence of very complex spectral changes and low S/N ratio.

Figure 3 shows the 2D synchronous (panel a) and asynchronous (panel b) correlation plots calculated from the retinal fingerprint spectra in Figure 2. The correlation analysis has been carried out after subtracting the first difference spectrum following light exposure. This procedure removes contributions from the static component of the spectra, corresponding to changes in infrared absorption that have developed during light exposure but have ceased to progress after the end of the illumination period. Therefore, only spectral components that keep evolving over the duration of the measurement are reported in the correlation plots. Peaks located along the diagonal of the synchronous plot (Figure 3a), the autocorrelation peaks, correspond to all the bands that change in the difference spectrum as a function of time. Peaks off the diagonal of both synchronous and asynchronous plots (Figure 3a,b) are due to the existence of correlation between changes at the corresponding wavenumber values. Off-diagonal peaks in the synchronous plot are due to correlation in-phase or with opposite phase (the phase difference is 0 or π). Off-diagonal peaks in the asynchronous plot are due to out-of-phase correlation (the phase difference is neither 0 nor π).

The plots are apparently very intricate, with a total of more than 400 maxima and minima in the synchronous plot (Figure 3a). To extract information from this complexity in a manageable form, we rely on the approach described by Massaro et al. to identify specific chromophores within a complex pattern of spectral changes.³⁰ Bands arising from the same chromophore display synchronous correlation and are perfectly in phase, giving rise to matching positive off-diagonal peaks in the synchronous correlation plot. In addition, bands arising from the same chromophore do not display any off-diagonal peaks in the asynchronous correlation plot because of the complete synchrony of their evolution. Therefore, the pairwise analysis of peak correlations allows the clustering of peaks arising from the

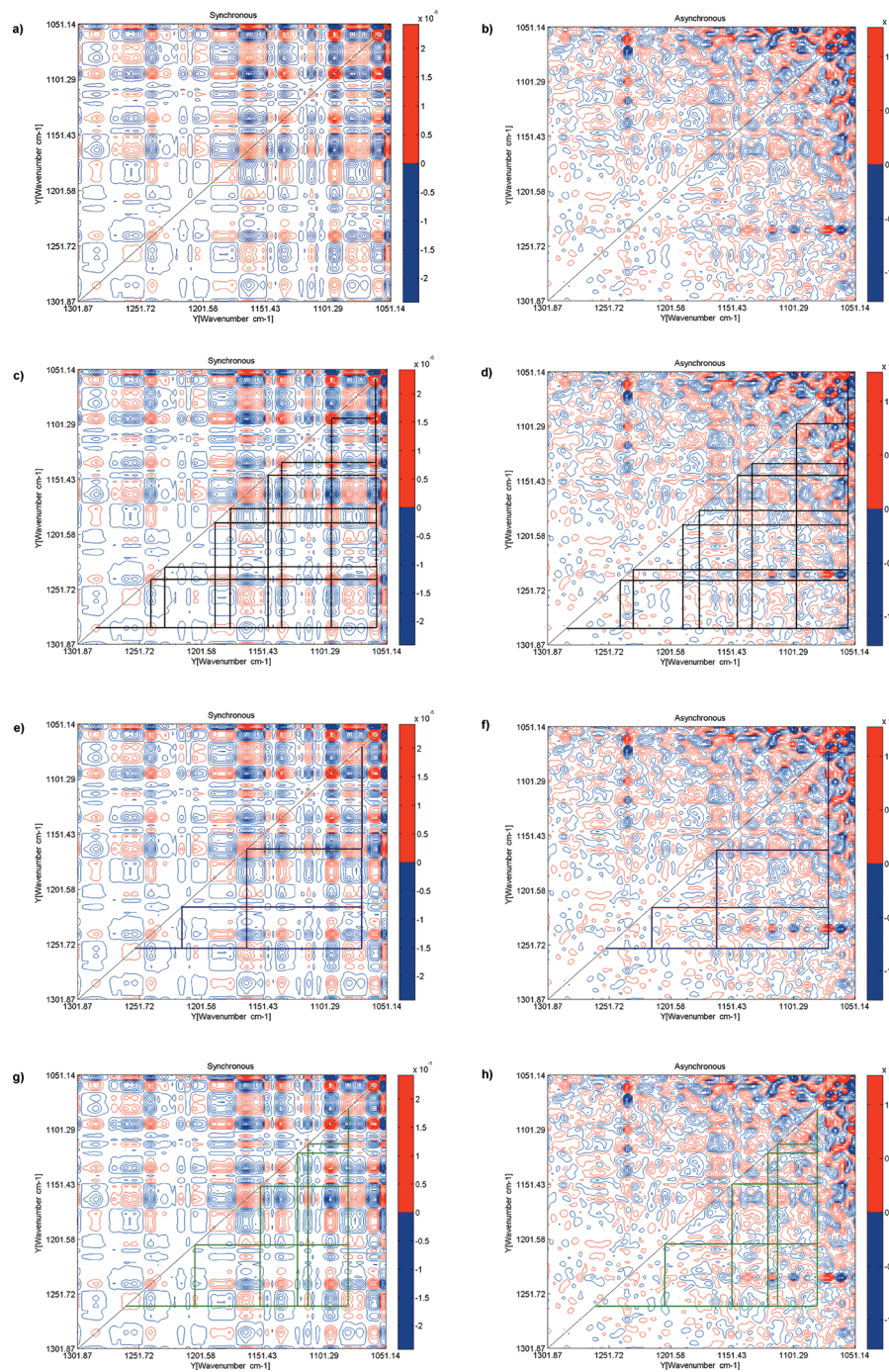


Figure 3. 2D correlation plots of differential spectra after photoexcitation. Detrended differential spectra collected during the first 600 s after photoexcitation were subject to 2D correlation analysis. The figure shows the resulting synchronous (a) and asynchronous (b) plots. Red contour curves correspond to positive values, and blue curves correspond to negative values. The lines of strong peaks at 1225 cm^{-1} in the asynchronous plot are due to a synchrotron oscillation. Plots c and d show a grid overlaid to the synchronous and asynchronous plots highlighting the peaks belonging to chromophore A. Peaks connected by the lines are all assigned to the same chromophore. Peaks from the same chromophore are characterized by strong correlation peaks off the diagonal in the synchronous plot. In the asynchronous plot, they show weak or null correlation and often correspond to positions off the diagonal where minima or saddle points are observed. Due to the symmetry properties of the plots around the diagonal, only one-half of the grid is represented. Peak positions are first determined from the synchronous plot and used to build the corresponding grid for the asynchronous plot. Plots e and f represent the corresponding grid for chromophore B while plots g and h show the grid for chromophore C.

same chromophore. It is important to note that in this context a single chromophore may actually correspond to more than one molecular species, provided that bands arising from all the contributing species change in full synchrony within the time

resolution of the experiment. Application of this analysis to the synchronous and asynchronous plots in Figure 3 allows the identification of groups of bands, each of them belonging to one of few different chromophores. Figure 3c–h gives a graphical

Table 1. List of Bands Assigned to the Main Chromophores Identified by 2D Correlation Spectroscopy^a

chromophore	band position (cm^{-1})										tentative assignment
A	1060	1095	1136	1147	1178	1190	1230	1242	1286		phospholipids or phosphoacetyl groups
B	1072	1165	1217		1254						all-trans retinal
C	1080	1115	1122	1153	1205	1261					meta-III

^a Band positions in the table correspond to the apparent maxima or minima in the synchronous 2D correlation plot from Figure 3a.

representation of the sets of correlated peaks for each chromophore by overlaying color coded grids to the synchronous and asynchronous plots. Peaks connected by the lines are all assigned to the same chromophore. Peaks from the same chromophore are characterized by strong correlation peaks off the diagonal in the synchronous plot. In the asynchronous plot, they show weak or null correlation and often correspond to positions off the diagonal where minima or saddle points are observed. Due to the symmetry properties of the plots around the diagonal, only one-half of the grid is represented. Peak positions are first determined from the synchronous plot and used to build the corresponding grid for the asynchronous plot. The large majority of the peaks (about 90%) in the synchronous plot of Figure 3a arise from the correlation of three sets of contributing bands, corresponding to as many chromophores that we label A, B, and C. As detailed above, each of these chromophores could correspond to more than one molecular species. The peaks of the latter chromophores are summarized in Table 1. In addition to these three chromophores, the only other additional bands are very weak contributions at 1109, 1211, and 1223 cm^{-1} . A detailed analysis of these weakly contributing chromophores with the same approach is not possible given the difficulty in detecting their contribution in the asynchronous spectrum, and they will not be discussed further.

An additional merit of this approach is to bring out weak bands buried in a complex background by taking advantage of their correlation with other bands of the same chromophore. The intensity of cross correlation peaks in the spectra of Figure 3a is dependent on both the intensity of the correlated peaks on the diagonal and their degree of correlation. Peaks arising from the same chromophore, even when weak, are characterized by strong correlation and give rise to appreciable off-diagonal peaks in the synchronous plot. Some examples are given by peaks at 1217, 1122, and 1106 cm^{-1} . These peaks are too weak to be observed as autocorrelation peaks, along the diagonal of Figure 3a. Nonetheless, their presence is revealed by the existence of a series of off-diagonal peaks due to correlation with other peaks of the same or of a different chromophore. This is an important additional piece of information which is very valuable in studying cellular processes, allowing the extraction of weaker contributions to the overall spectrum.

To validate the method, we compare the IR spectral changes identified in the intact cell with the existing knowledge on rod cell physiology. Rod cells are one of the best studied cellular systems, and a wealth of information is available concerning their biochemistry and the properties of their molecular components. The literature concerning spectroscopic studies of rhodopsin and associated biomolecules is particularly rich, providing a valuable comparison.

Chromophore A displays absorptions at 1060, 1095, 1136, 1147, 1178, 1190, 1230, 1242, and 1286 cm^{-1} . The 1060 cm^{-1} and 1095 cm^{-1} diagonal peaks in the synchronous correlation plot are among the most intense in the plot, indicating a major

contribution of this chromophore to the evolving spectral bands. Band position and relative intensities suggest that this chromophore can be identified with a phospholipid species. 1240 cm^{-1} and 1090 cm^{-1} are characteristic frequencies for the antisymmetric stretching mode of the phosphodiester group, $\nu_{\text{as}}(\text{PO}_3^-)$, and the symmetric stretching mode $\nu_s(\text{PO}_3^-)$, respectively.⁴⁵ The assignment to more than one phospholipid species is also possible provided that their absorbance changes are all in synchrony, such as in the case of a reorganization of membrane bilayer structure. The FT-IR spectra of the intact photoreceptor membrane display prominent peaks around 1065, 1070, 1095, and 1240 cm^{-1} that are dominated by lipid contributions and disappear after delipidation,⁴⁶ supporting the assignment of chromophore A to the lipid complement of the ROS. The observation of light induced changes in the phospholipids of the ROS has also been reported by the use of spin-label techniques.³⁴

A strong fingerprint band at 1238 cm^{-1} is commonly assigned to the 11-cis-retinal of dark Rho.⁴⁷ However, this band is expected to dominate the fingerprint region in difference spectra recorded after illumination of rhodopsin whereas the bands of chromophore A are dominated by the peaks at 1060 cm^{-1} and 1095 cm^{-1} . Although it is still possible that 11-cis-retinal contributes to this chromophore absorption, this would be only a minority contribution. The decrease of absorption from 11-cis-retinal is expected to have developed mostly during the illumination phase.

Outside of the retinal fingerprint region, a strong band at 1726 cm^{-1} (Supporting Information, Figure S3,A,B) evolves in synchrony with the other bands of this chromophore. In the region between 1400 and 1600 cm^{-1} (Supporting Information, Figure S3,A,B), synchrony can be ascertained only with a band at 1403 cm^{-1} ; the presence of synchronous correlations between residual atmospheric water vapor bands prevents additional assignments. The range of 1710–1745 cm^{-1} contains the absorption bands of carbonyl groups from phospholipid ester bonds, while around 1400 cm^{-1} methyl and methylene deformations absorb, in agreement with the assignment of chromophore A to a phospholipid. The observation of changes in lipid absorption bands induced by photoexcitation is in agreement with the interpretation of changes in macroscopic optical properties of photoexcited ROS as arising from lipid reorganization.^{34,48} The time evolution of the absorption changes, over the range of 30 min, is also in agreement with the time evolution of the SSc trace as shown in Figure 1.

Chromophore B displays absorptions at 1072, 1165, 1217, and 1254 cm^{-1} . A weakly changing band at 1205 cm^{-1} is also possibly assigned to this chromophore, although the asynchronous plot is unclear in this respect. An assignment of the 1205 cm^{-1} band to chromophore C is also possible. The band at 1168 cm^{-1} dominates the spectrum of this chromophore according to the intensity of its autocorrelation peak. Bands at 1167, 1202, and 1255 cm^{-1} have been associated to the bound retinal in dark state bacteriorhodopsin,⁴⁹ with an all-trans

conformation, suggesting that a similar assignment could be valid for chromophore B. $\nu_{C10-C11}$ is the strongest peak in the spectrum of all-trans retinal in solution (see Supporting Information, Figure S2), as observed in chromophore B. The strong water absorption around 1640 cm^{-1} prevents us from observing the presence or absence of the $\nu_{C=N}$ band from the Schiff-base bond of the retinal to the protein. Therefore, we cannot use this marker to confirm whether we are observing an opsin-bound form of all-trans retinal or a cytoplasmic free form. The time evolution of chromophore B, as measured from the changes of the two strongest peaks at 1168 cm^{-1} and 1072 cm^{-1} , occurs over 20–30 min, similar to what has been reported for the release of the chromophore in single rods of *B. bufo* from spectrophotometric measurements.⁵² This is also the time evolution of retinal release as reported from measurements of intrinsic tryptophan fluorescence.⁵⁰ On this basis, we propose that this chromophore be identified with a conformational isomer of all-trans retinal formed after release from opsin, either a cytoplasm free species or a Schiff-base formed by retinal condensation with an amine group exposed to the cytoplasm.

Chromophore C displays absorptions at 1080, 1115, 1122, 1153, 1205, and 1261 cm^{-1} . Overall, this chromophore contributes the least to the 2D correlation plots, having relatively weak autocorrelation peaks, and is likely to be a species that is present only at low concentrations or subject to small changes. Correlation plots calculated using spectra recorded after 300 s from illumination do not show this chromophore any longer (see Supporting Information, Figure S4,A,B), indicating that this is probably a low-accumulating intermediate that decays during the first five minutes of the measurement. The bands at 1153 cm^{-1} and 1205 cm^{-1} are in agreement with the values reported for bands belonging to the fingerprint region of intermediate meta-III.^{22,38} The bands at 1122, 1115, and 1080 cm^{-1} also have equivalents in the published fingerprint spectra of meta-III,³⁸ although an accurate comparison is not fully viable since the authors did not report peak positions. The only major component of the fingerprint of meta-III that is not clearly observed in the synchronous plots of Figure 2 is the band at $\sim 1180\text{ cm}^{-1}$,³⁸ which overlaps with the band of chromophore A at 1178 cm^{-1} . Comparison with the corresponding region in the asynchronous plots does suggest the presence of additional weak overlapping bands. The lifetime of Chromophore C does indeed correspond to the lifetime of meta-III measured by spectrophotometry in single rod cells. Another possibility is the assignment to the ATP/ADP pair, based on expected concentration and presence of contributions of this chromophore in this spectral region. However, the FT-IR spectral response to ATP hydrolysis has been reported by Kim et al. None of the identified chromophores display absorption bands corresponding to ATP hydrolysis.^{51,52} Although isotopic substitution experiments would be necessary for confirming it, we suggest an assignment of chromophore C to meta-III. The assignment of chromophores to specific molecular species is summed up in Table 1.

The amount of information which can be extracted from the generalized 2D plots shown in Figure 3 is remarkable, considering the complexity of the system under study. Part of this arises from the possibility of the use of 2D correlations to assign bands to specific chromophores, as shown in this work. The assignment would be unfeasible if the information contained in complex one-dimensional spectra was used, particularly in the absence of parallel information from experiments of isotopic substitution or chromophore deletion. Another benefit of the use of 2D

correlations arises from the possibility to improve the spectral resolution of components. As with other multidimensional spectroscopic approaches, the improvement in resolution arises from the possibility of spreading bands onto a 2D plot based on their different response to a perturbation or their different evolution as a function of a parameter. In an evolving cellular system, this effect is ascribed to the different rate of change of individual molecules, which leads to different degrees of correlation between them. In this work, the resolution of the peaks at 1153 cm^{-1} and 1165 cm^{-1} in Figure 3 can be attributed to their different time courses and would not have been feasible in single time-resolved spectral traces. A third major advantage of 2D correlation analysis is the use of synchronous plots for the recovery of weak absorption changes that are at or below noise level in one-dimensional spectra. This feature is due to the small synchronous correlation in Gaussian noise. It was recently suggested⁵³ that such an application to subcellular spectromicroscopy could lead to the recovery of weak spectral changes that would otherwise be buried in noise. In this work, the observation of several bands assigned to chromophore A would have been unfeasible in one-dimensional spectra, in particular in the noisier region below 1100 cm^{-1} . Chromophore C would have been completely undetected without 2D correlation. To our knowledge, this is the first verification of the viability of such an approach to subcellular measurements.

It is important to note that the removal of baseline effects from time-resolved spectra is critical for the successful application of 2D correlation analysis. In this context with baseline effects, we mean all variations in the spectrum that are not due to the changes in sample absorption that are the focus of the investigation. Examples reported in this work are optical effects due to variations in sample geometry and in sample refractive index. Failure to satisfy this condition would result in synchronous and asynchronous plots where baseline changes would correlate with the spectroscopic changes of interest, giving rise to broad and complex features in correlation spectra. To be able to assign peaks to the same chromophore, as we have shown, it is of critical importance being able to confirm a lack of asynchronous correlation between peaks. This is carried out in practice by identifying saddle points or minima in the asynchronous plot and would be impossible in the presence of strong baseline changes. It is also to be noted that the baseline subtraction protocol should be carefully chosen on a case-by-case basis according to what is the origin of baseline variations.

CONCLUSIONS

We show that synchrotron FT-IR spectromicroscopy allows one to detect weak spectroscopic changes in an evolving cellular system. We characterize the changes induced by photoexcitation in the mid-infrared spectral region by resolving them into variations in refraction/scattering, associated to changes of the real refractive index of the ROS, and variations in absorption, associated to changes of the imaginary refractive index of the ROS. Their time course is consistent with a light-induced reorganization of the ROS, as inferred from comparison with published experiments using a variety of techniques. We show that the technique allows us to measure changes in absorbance of 10^{-3} to 10^{-4} au per minute in an individual ROS.

The application of 2D correlation analysis to the spectral traces allows identification of bands arising from the same chromophore, thus providing a valuable tool to reveal

contributions from specific molecular species in the complex difference spectra of a cellular system. In addition, it allows us to recover weak absorption changes that would have gone undetected in the analysis of one-dimensional spectra.

We believe that the overall strategy used for these experiments goes beyond the specific case of retinal rod cells and is of general utility for the quantitative study of time-resolved changes in cellular systems. In particular, the possibility of clearly identifying the bands from specific chromophores allows infrared spectro-microscopy of cells to progress beyond the common practice of “functional group analysis and mapping”, which is the state-of-the-art in current applications. A traditional use of FT-IR spectroscopy has been the identification of specific chromophores via a “fingerprinting” approach, whereby the complex spectral pattern arising from one molecule is used as a unique identifier. The application of this approach is elementary for simple systems, with a limited number of dominant components. However, it is often unreliable in complex samples such as cells, in which only a few stronger bands can be observed and only for the most abundant molecules. Showing how 2D correlation analysis can expand the complement of observable bands, we provide a tool to extend the application of infrared “fingerprinting” to cellular dynamics. When one is able to identify bands from specific molecules and extract weak ones from a noisy background, it opens the way to the observation of detailed structural changes over time, the study of the relationship between structure and dynamics in living cells.

■ ASSOCIATED CONTENT

S Supporting Information. Additional information as noted in text. This material is available free of charge via the Internet at <http://pubs.acs.org>.

■ AUTHOR INFORMATION

Corresponding Author

*E-mail: luca.quaroni@psi.ch.

■ ACKNOWLEDGMENT

We thank Kira Goff and Ron Zvarich, of the Canadian Light Source, for design of the sample holder. We also thank Tim May and Tor Pedersen of the Canadian Light Source and Jörg Wambach and Philippe Lerch of the Paul Scherrer Institut for construction and maintenance of the respective beamlines. 9-cis-Retinal was donated by the group of Rosalind Crouch at the National Eye Institute, part of the National Institutes of Health (USA). The project was supported by funds from the Canadian Light Source and the Swiss Light Source. Experiments were performed at beamline X01DC of the Swiss Light Source and Beamline 01B1-1 at the Canadian Light Source. The Canadian Light Source is supported by the Natural Sciences and Engineering Research Council of Canada, the National Research Council Canada, the Canadian Institutes of Health Research, the Province of Saskatchewan, Western Economic Diversification Canada, and the University of Saskatchewan.

■ REFERENCES

- (1) Berthomieu, C.; Hienerwadel, R. *Photosynth. Res.* **2009**, *101*, 157–170.
- (2) Noguchi, T.; Berthomieu, C. *Adv. Photosynth. Respir.* **2005**, *22*, 367–387.
- (3) Gerwert, K. *Biol. Chem.* **1999**, *380*, 931–935.
- (4) Wetzel, D. L.; LeVine, S. M. *Science* **1999**, *285*, 1224–1225.
- (5) Levin, I. W.; Bhargava, R. *Annu. Rev. Phys. Chem.* **2005**, *56*, 429–474.
- (6) Chalmers, J. M. In *Biomedical Applications of Synchrotron Infrared Spectromicroscopy*; Moss, D., Ed.; Royal Society of Chemistry: Cambridge, 2011; Vol. 11, pp 29–66.
- (7) Quaroni, L.; Zlateva, T. *Analyst (Cambridge, U.K.)* **2011**, *136*, 3219–3232.
- (8) Holman, H.-Y. N.; Bechtel, H. A.; Hao, Z.; Martin, M. C. *Anal. Chem.* **2010**, *82* (21), 8757–8765.
- (9) Jamin, N.; Dumas, P.; Moncuit, J.; Fridman, W. H.; Teillaud, J. L.; Carr, G. L.; Williams, G. P. *Proc. Natl. Acad. Sci. U. S. A.* **1998**, *95*, 4837–4840.
- (10) Zhao, R.; Quaroni, L.; Casson, A. G. *Analyst* **2010**, *135*, 53–61.
- (11) Carr, G. L.; Miller, L. M.; Dumas, P. In *Biomedical Applications of Synchrotron Infrared Spectromicroscopy*; Moss, D., Ed.; Royal Society of Chemistry: Cambridge, 2011; Vol. 11, pp 226–259.
- (12) Nasse, M. J.; Walsh, M. J.; Mattson, E. C.; Reininger, R.; Kajdacsy-Balla, A.; Macias, V.; Bhargava, R.; Hirschmugl, C. J. *Nat. Methods* **2011**, *8*, 413–416.
- (13) Quaroni, L.; Zlateva, T.; Bedolla, D.; Massaro, S.; Torre, V. *ChemPhysChem* **2008**, *9*, 1380–1382.
- (14) Goff, K. L.; Quaroni, L.; Wilson, K. E. *Analyst* **2009**, *134*, 2216–2219.
- (15) Baylor, D. *Proc. Natl. Acad. Sci. U. S. A.* **1996**, *93*, 560–565.
- (16) Stryer, L. *Proc. Natl. Acad. Sci. U. S. A.* **1996**, *93*, 557–559.
- (17) Hamer, R. D.; Nicholas, S. C.; Tranchina, D.; Lamb, T. D.; Jarvinen, J. L. P. *Vis. Neurosci.* **2005**, *22*, 417–436.
- (18) Papermas, D. S.; Dreyer, W. J. *Biochemistry (Moscow)* **1974**, *13*, 2438–2444.
- (19) Hamm, H. E.; Bownds, M. D. *Biochemistry (Moscow)* **1986**, *25*, 4512–4523.
- (20) Stryer, L. *Harvey Lectures*; The Harvey Society: New York, 1993; *87*, pp 129–143.
- (21) Arshavsky, V. Y.; Lamb, T. D.; Pugh, E. N. *Annu. Rev. Physiol.* **2002**, *64*, 153–187.
- (22) Ritter, E.; Elgeti, M.; Hofmann, K. P.; Bartl, F. J. *J. Biol. Chem.* **2007**, *282*, 10720–10730.
- (23) Vogel, R.; Siebert, F. *Biopolymers* **2003**, *72*, 133–148.
- (24) Harrington, P. d. B.; Urbas, A.; Tandler, P. J. *Chemom. Intell. Lab. Syst.* **2000**, *50*, 149–174.
- (25) Hofmann, K. P.; Schleicher, A.; Emeis, D.; Reichert, J. *Biophys. Struct. Mech.* **1981**, *8*, 67–93.
- (26) Hofmann, K. P.; Schleicher, A.; Emeis, D.; Reichert, J. *Biophys. Struct. Mech.* **1981**, *7*, 339–339.
- (27) Davis, B. J.; Carney, P. S.; Bhargava, R. *Anal. Chem.* **2010**, *82*, 3474–3486.
- (28) Davis, B. J.; Carney, P. S.; Bhargava, R. *Anal. Chem.* **2010**, *82*, 3487–3499.
- (29) Davis, B. J.; Scott Carney, P.; Bhargava, R. *Anal. Chem.* **2011**, *83*, 525–532.
- (30) Massaro, S.; Zlateva, T.; Torre, V.; Quaroni, L. *Anal. Bioanal. Chem.* **2008**, *390*, 317–322.
- (31) Leibrock, C. S.; Reuter, T.; Lamb, T. D. *Vision Res.* **1994**, *34*, 2787–2800.
- (32) Kolesnikov, A. V.; Golobokova, E. Y.; Govardovskii, V. I. *Vis. Neurosci.* **2003**, *20*, 249–265.
- (33) Kennedy, M. J.; Lee, K. A.; Niemi, G. A.; Craven, K. B.; Garwin, G. G.; Saari, J. C.; Hurley, J. B. *Neuron* **2001**, *31*, 87–101.
- (34) Hessel, E.; Muller, P.; Herrmann, A.; Hofmann, K. P. *J. Biol. Chem.* **2001**, *276*, 2538–2543.
- (35) Goff, K. L.; Quaroni, L.; Wilson, K. E.; Pedersen, T. *AIP Conf. Proc.* **2009**, *1214*, 54–56.
- (36) Lüdeke, S.; Fonfria, V. A. L.; Siebert, F.; Vogel, R. *Biopolymers* **2006**, *83*, 159–169.

- (37) Vogel, R.; Siebert, F.; Mathias, G.; Tavan, P.; Fan, G. B.; Sheves, M. *Biochemistry (Moscow)* **2003**, *42*, 9863–9874.
- (38) Bartl, F. J.; Vogel, R. *Phys. Chem. Chem. Phys.* **2007**, *9*, 1648–1658.
- (39) Menon, S. T.; Han, M.; Sakmar, T. P. *Physiol. Rev.* **2001**, *81*, 1659–1688.
- (40) Bartl, F. J.; Ritter, E.; Hofmann, K. P. *J. Biol. Chem.* **2001**, *276*, 30161–30166.
- (41) Vogel, R.; Lüdeke, S.; Radu, I.; Siebert, F.; Sheves, M. *Biochemistry (Moscow)* **2004**, *43*, 10255–10264.
- (42) Mason, W. T.; Fager, R. S.; Abrahamson, E. W. *Biochemistry (Moscow)* **1973**, *12*, 2147–2150.
- (43) Hessel, E.; Herrmann, A.; Muller, P.; Schnetkamp, P. P. M.; Hofmann, K. P. *Eur. J. Biochem.* **2000**, *267*, 1473–1483.
- (44) Noda, I. *Front. Mol. Spectrosc.* **2009**, 367–381.
- (45) Rothschild, K. J.; Sanches, R.; Clard, N. A.; Lester, P. In *Methods Enzymol.*; Academic Press, 1982; Vol. 88, pp 696–714.
- (46) Rothschild, K. J.; Degrip, W. J.; Sanches, R. *Biochim. Biophys. Acta* **1980**, *596*, 338–351.
- (47) Vogel, R.; Siebert, F. *J. Biol. Chem.* **2001**, *276*, 38487–38493.
- (48) Isele, J.; Sakmar, T. P.; Siebert, F. *Biophys. J.* **2000**, *79*, 3063–3071.
- (49) Gerwert, K.; Siebert, F. *EMBO J.* **1986**, *5*, 805–811.
- (50) Heck, M.; Schadel, S. A.; Maretzki, D.; Bartl, F. J.; Ritter, E.; Palczewski, K.; Hofmann, K. P. *J. Biol. Chem.* **2003**, *278*, 3162–3169.
- (51) Barth, A.; Mantele, W. *Biophys. J.* **1998**, *75*, 538–544.
- (52) Parke, C. L.; Wojcik, E. J.; Kim, S.; Worthylake, D. K. *J. Biol. Chem.* **2010**, *285*, 5859–5867.
- (53) Quaroni, L.; Normand, E. *AIP Conf. Proc.* **2009**, *1214*, 66–68.